Developmental "awakening" of primary motor cortex to the sensory consequences of movement

James C. Dooley[1,4] and Mark S. Blumberg*[1, 2, 3, 4, 5]

[1]Department of Psychological & Brain Sciences, University of Iowa, Iowa City, IA 52242, USA
[2]Interdisciplinary Graduate Program in Neuroscience, University of Iowa, Iowa City, IA 52245, USA
[3]Department of Biology, University of Iowa, Iowa City, IA, 52242 USA
[4]DeLTA Center, University of Iowa, Iowa City, IA 52242 USA
[5]Iowa Neuroscience Institute, University of Iowa, Iowa City, IA 52242 USA

Corresponding author: Mark S. Blumberg (mark-blumberg@uiowa.edu)

SUMMARY

Before primary motor cortex (M1) develops its motor functions, it behaves like a somatosensory area. Here, by recording from neurons in the forelimb representation of M1 in postnatal day (P) 8-12 rats, we demonstrate a rapid change in the types of movements that trigger sensory responses. At P8-10, M1 neurons respond overwhelmingly to sleep-related twitches of the forelimb, but the same neurons do not respond to forelimb movements when the animal is awake. Then, only two days later, M1 neurons suddenly respond to feedback from wake movements; this transition results from a change in sensory gating by the external cuneate nucleus. Also, at P12, the onset of local cortical inhibition leads to fewer M1 neurons responding to twitches; pharmacological disinhibition unmasks the more robust twitch responsiveness observed at P8. Thus, M1 initially establishes a somatosensory framework that lays a foundation for later-emerging motor control and plasticity.

Keywords: Development, motor control, motor plasticity, external cuneate nucleus, myoclonic twitching, REM sleep, neurophysiology, sensorimotor integration

INTRODUCTION

Primary motor cortex (M1) assumes its role in motor production and motor learning relatively late in development (Chakrabarty and Martin, 2000; Flament et al., 1992; Martin et al., 2005; Muller et al., 1991; Nezu et al., 1997; Olivier et al., 1997; Young et al., 2012). For example, using intracortical microstimulation in anesthetized rats, movements could not be evoked in M1 until postnatal day (P) 35 (Young et al., 2012). It is not understood why M1 shows such protracted development or how M1 functions before it assumes its "motor identity." One possibility is that M1 first develops a sensory framework upon which its later-emerging motor functions rest (Bruce and Tatton, 1980; Chakrabarty and Martin, 2005). However, little is known about the early development of sensory responses in M1 neurons, and the process by which these early neural responses set the stage for M1's role in motor learning and plasticity.

Beginning early in development, M1 neurons respond to externally generated (i.e., exafferent) proprioceptive stimulation (An et al., 2014; Asanuma, 1981; Tiriac and Blumberg, 2016). In addition, M1 neurons respond to proprioceptive feedback from self-generated movements (i.e., reafference). For example, in adults, M1 neurons strongly respond to reafference from wake movements (Asanuma, 1981; Fetz et al., 1980; Georgopoulos et al., 1982; Goldring and Ratcheson, 1972; Hatsopoulos and Suminski, 2011; Schroeder et al., 2017). In contrast, in week-old rats, M1 neurons do not respond to reafference from wake movements; instead, they are strongly driven by sensory feedback arising from myoclonic twitches—the jerky movements produced abundantly and exclusively during active (REM) sleep (Tiriac et al., 2014). With respect to the forelimb, suppression of wake-related reafference is due to selective inhibition within the external cuneate nucleus (ECN), a medullary nucleus that receives primary proprioceptive afferents from forelimb muscle spindles and conveys that afferent information to downstream structures (Boivie and Boman, 1981; Campbell et al., 1974). Consequently, in early development, it appears that M1 neurons are "blind" to the proprioceptive consequences of wake movements.

In adults, proprioceptive input to M1 arrives directly from thalamus but can also arrive indirectly through primary somatosensory cortex (S1; Asanuma, 1981). Contemporary theories of M1's role in motor learning assume it has access to this proprioceptive input, permitting continuous monitoring of limb position and updating of motor commands (Mathis et al., 2017; Miri et al., 2017). These theories take for granted both M1's role in producing movements and the availability of reafference from those movements, neither of which pertains to M1 early in development. However, as development progresses and M1 assumes its motor functions, there must come a time when M1 neurons begin to respond to proprioceptive feedback from wake movements. How M1 transitions from its initial sensory identity to its adult motor identity has never been addressed. What is known is that in rats intracortical microstimulation of M1 neurons at P13 can evoke

movement, but only after local disinhibition with the $GABA_A$ antagonist, bicuculline (Young et al., 2012). That this effect was not observed one day earlier suggests that P12 marks a transition in M1's functional development.

By recording extracellularly from the forelimb representation of M1 in unanesthetized P8-12 rats as they cycled between sleep and wake, we demonstrate several key events in the early development of M1 sensory processing. First, consistent with previous studies (Tiriac and Blumberg, 2016; Tiriac et al., 2014), we find that M1 neurons at P8-10 are responsive to reafference from twitches, but not wake movements. Between P10 and P12, this pattern changes such that M1 neurons now respond to reafference from wake movements, but less often to twitches. Because M1 neurons at all ages respond to external stimulation (i.e., exafference), the developmental change must be due to specific changes in the processing of input arising from self-generated movements. Next, we show that the change results from two separate developmental events around P12: (i) an upstream change in the gating of wake-related reafference in the ECN and (ii) the sudden onset of inhibitory circuits within M1 that suppresses twitch-related reafference. Together, these events signal a dramatic shift in M1 sensory processing that constitutes an "awakening" to the sensory consequences of movement at a time when motor outflow from M1 is just beginning to emerge.

RESULTS

We recorded neural activity from the forelimb representation of M1 in head fixed, unanesthetized rats each day from P8 to P12 (P8: n = 10, 160 neurons; P9: n = 9, 112 neurons; P10: n = 8, 123 neurons; P11: n = 15, 197 neurons; P12: n = 7, 165 neurons; see Table S1 for more details) using 4-shank silicon depth electrodes (Fig. S1A). M1 neuronal activity, as well as nuchal, forelimb, and hindlimb electromyographic (EMG) activity, was recorded for 30 min as the pups cycled freely between sleep and wake (Fig. 1A). We confirmed electrode placement in the forelimb representation of M1 through exafferent stimulation of the forelimb as well as subsequent staining of flattened, tangentially sectioned brains for cytochrome oxidase (CO). Sectioned brains revealed that all recording sites were restricted to agranular cortex immediately medial to the forelimb representation of S1 (Fig. 1B-D). In a subset of coronally sectioned brains, recording depth was confirmed to be in the primary thalamic recipient layers of agranular cortex (Bopp et al., 2017), spanning layers 3-5 (Fig. S1).

Rapid Developmental Change Sensory Responsiveness of M1 Neurons

As reported previously in P8 rats (Tiriac and Blumberg, 2016; Tiriac et al., 2014), neurons in the forelimb representation of M1 exhibited more activity during periods of active sleep than during periods of wake (Fig. 2A, left). Perievent histograms revealed

that neuronal activity in M1 during active sleep clustered around forelimb myoclonic twitches, but not wake movements of the forelimb (Fig. 2A, right). The pattern of neural activity at P9 and P10 largely resembled that at P8. However, at P11, M1 neurons were substantially more active during wake (Fig. 2B, left), with increased activity after wake movements in addition to a continued response to twitches (Fig. 2B, right). By P12, M1 neurons were continuously active during sleep and wake (Fig. 2C, left). Similar to P11, M1 activity increased after forelimb wake movements at P12, but no longer increased after twitches (Fig. 2C, right). Notably, of the 757 cortical neurons from which we recorded, not one exhibited increased activity before twitches or wake movements, thus providing the strongest evidence to date that M1 is not yet involved in the production of spontaneous movement at these ages (but see An et al., 2014).

Between P8 and P12, we observed an age-related decrease in the number of forelimb twitches produced per unit time (Fig. S2A, $F_{(4,44)} = 11.4$, $P < 0.0001$), consistent with previous reports (Marcano-Reik et al., 2010), but did not observe a change in the number of wake movements ($F_{(4,44)} = 1.1$, $p = 0.37$). Importantly, because the profiles of EMG activity associated with twitches and wake movements did not change with age (Fig. S2B), the age-related change in the reafferent responses of M1 neurons to twitches and wake movements cannot be attributed to differences in the kinematics of these movements. Thus, the developmental transition of M1 neurons from being predominantly twitch-responsive to predominantly wake-responsive is due to a state-dependent change in the processing of reafference, rather than a change to the movements themselves.

Developmental Shift in the Population Characteristics of Neuronal Responses in M1

To determine whether individual neurons were twitch- or wake-responsive, perievent histograms triggered on twitches or wake movements were constructed for each isolated M1 neuron. We then fit perievent histograms to models of idealized M1 neuronal responses using custom-written MATLAB code. Twitches, being discrete movements, were fit to a symmetrical Gaussian function (Fig. 3A); in contrast, wake movements were fit to an asymmetrical function comprising a Gaussian with an exponential decay (Fig. 3B). We used these models to perform regression analyses on each neuron, assigning each to a response category based on its adjusted r^2 values. Using a threshold of adj. $r^2 = 0.35$, we classified all M1 neurons as either unresponsive (both twitch and wake adj. $r^2 \leq 0.35$) or responsive (twitch and/or wake adj. $r^2 > 0.35$). A representative unresponsive neuron, as well as representative responsive neurons from each of the three possible classifications (twitch-responsive, wake-responsive, twitch- and wake-responsive) are shown in Fig. 3C.

The choice of a threshold of 0.35 to define unresponsive and responsive neurons was justified by comparing the mean change in firing rate (in relation to baseline) across neuron types. Unresponsive neurons did not exhibit increased firing rates after forelimb twitches or wake movements at any age (Fig. S3A; grey squares), whereas responsive neurons exhibited increased activity after movements at all ages (Fig. S3A; blue, purple, and red squares). There was no age-related difference in the percentage of neurons classified as unresponsive (χ^2_4= 5.3, p = 0.26; Fig. S3B).

Scatterplots of adj. r^2_{twitch} vs. adj. r^2_{wake} for each neuron show a developmental shift in the neural population responses to twitches and wake movements, particularly between P10 and P12 (Fig. 4A). Whereas most responsive neurons at P8 and P9 (and, to a lesser extent, P10) occupy the twitch-responsive quadrant (top-left, blue), by P11 most of the responsive neurons have shifted to the twitch- and wake-responsive quadrant (top-right, purple). By P12 the population has shifted again, with most responsive neurons now occupying the wake-responsive quadrant (bottom-right, red). This population-level shift in responsivity is supported quantitatively, with responsive neurons showing a significant decrease in adj. r^2_{twitch} from P8 to P12, the most dramatic decrease being between P11 and P12 (Fig. 4B, blue bars). Correspondingly, the adj. r^2_{wake} increased from P8 to P12 (Fig. 4B, red bars). The age-related reversal in responsiveness is most visually apparent as a change in the percentage of responsive neurons that are twitch-responsive, twitch- and wake-responsive, and wake-responsive across age (Fig. 4C). Importantly, all responsive neurons also responded to exafferent stimulation of the forelimb (Fig. S3A; green lines), thus demonstrating that the developmental changes in sensory processing by M1 neurons are specifically related to feedback from self-generated movements.

The decreased neuronal response to twitches between P8 and P12 is accompanied by an apparent increase in somatotopic refinement. In support of this, twitch-responsive neurons exhibited developmental increases in peak firing rate, narrower response tuning, and decreased latency (Fig. S4, top; Table S2). Further, P11 and P12 twitch-responsive neurons responded more consistently after a twitch than twitch-responsive neurons at P8-10. Thus, although fewer neurons responded to twitches at P12, the remaining twitch-responsive neurons were more homogeneous, suggestive of a more precise representation. Finally, Gaussian-exponential fits of wake-responsive neurons did not show similar developmental trajectories (Fig. S4, bottom; Table S2), most likely because wake movements are inherently more noisy and variable than twitches.

Developmental Onset of Wake-Related Reafference in the ECN

The ECN acts as a sensory gate that selectively blocks wake-related reafference at P8-10 (Fig. 5A; Tiriac and Blumberg, 2016). Because the unresponsiveness of M1 neurons to wake-related reafference is attributable to upstream blockade in the ECN, we

hypothesized that the sudden emergence of wake movement responses at P11-12 is likewise attributable to a change at the level of the ECN (Fig. 5B). We tested this hypothesis by comparing ECN neuronal activity in unanesthetized, head fixed rats at P8-9 (hereafter P9; n=6 pups, 16 neurons) and P11-12 (hereafter P12; n=7 pups, 20 neurons; Fig. S5A,B; Table S1).

As described earlier (Tiriac and Blumberg, 2016), we observed robust responses in P9 ECN neurons to forelimb twitches, but not wake movements (Fig. 5C). At P12, however, ECN neurons responded both to twitches and wake movements (Fig. 5D). Thus, ECN neurons were also fit to Gaussian and Gaussian-exponential functions (see Fig. 3A, B). Representative fits of P9 and P12 ECN neurons are shown in Fig. S5C. ECN neuron responses were similar in shape to M1 neuron responses, but with shorter latencies and narrower widths (see Table S2). At P9, ECN neurons were predominantly twitch-responsive (Fig. 6A left; 11 of 16 neurons); in contrast, at P12, neurons were predominantly twitch- and wake-responsive (Fig. 6A right; 15 of 20 neurons). P9 and P12 ECN neurons were similarly twitch-responsive (Fig. 6B, blue bars; t_{34} = 1.8, P = 0.09), but P12 neurons were significantly more wake-responsive than P9 neurons (Fig. 6B, red bars; t_{34} = 2.9, P = 0.006), resulting in very different distributions at these ages (Fig. 6C). Thus, we concluded that the increase in wake responsiveness of M1 neurons at P11 is due to a state-dependent change in sensory gating in the ECN.

Local M1 Disinhibition at P12 Unmasks Twitch-Related Activity

At P12, neurons in the ECN continue to respond to twitch-related reafference; accordingly, the loss of twitch-related reafference in M1 neurons cannot be attributed to the ECN, thus implicating a downstream structure. One possibility is that the change occurs within M1 itself.

The second postnatal week is a period when cortical inhibitory circuits become functionally active (Ben-Ari et al., 2007). Thus, we hypothesized that state-dependent activation of local GABAergic interneurons mediates the observed decrease in the twitch responsiveness of M1 neurons at P12 (Fig. 7A). To test this hypothesis, we recorded from M1 neurons at P12 before and after injection of the $GABA_A$ antagonist, bicuculline (n=6 pups, 99 neurons) or saline (n=6 pups, 107 neurons; Table S1). We confirmed that electrodes were located within the forelimb representation of M1 and that drug diffusion was largely confined to the area immediately surrounding the electrode (Fig. 7B,C).

Perievent histograms of twitch and wake responses before (Pre) and after (Post) injection were fit to Gaussian and Gaussian-exponential functions. Representative neural activity is illustrated in Fig. S6. For saline-injected pups, scatterplots of adj. r^2_{twitch} and adj. r^2_{wake} replicate our previous finding: P12 M1 neurons were predominantly

wake-responsive, occupying the wake-responsive (bottom right, red) quadrant of the scatterplots (Fig. 7D, top row). Likewise, before the injection of bicuculline, M1 neurons were predominantly wake-responsive (Fig. 7D, bottom left). However, after injection of bicuculline, there was a dramatic increase in twitch-responsiveness of the previously wake-responsive neurons, shifting the population activity to the twitch- and wake-responsive (top right, purple) quadrant of the scatterplot (Fig. 7D, bottom right). Quantitatively, as shown in Fig. 7E, M1 neurons exhibited increased adj. r^2_{twitch} after injection of bicuculline (Z_{65} = 6.8, P < 0.0001), with no corresponding change in adj. r^2_{awake} (Z_{65} = 1.8, p = 0.08). Saline injection had no effect on adj. r^2_{twitch} and adj. r^2_{awake}. Thus, local disinhibition in M1 is sufficient to unmask twitch-related reafference, resulting in neural activity that exhibits a uniquely high percentage of twitch- and wake-responsive neurons (Fig. 7F). In other words, the disinhibited M1 neuronal activity at P12 combines the response profiles of wake-responsive M1 neurons and twitch-responsive ECN neurons.

DISCUSSION

To better understand developmental changes in how M1 neurons process sensory feedback from self-generated movements, we characterized their reafferent responses to twitches and wake movements. Consistent with previous reports in P8 rats, we found that M1 neurons were overwhelmingly responsive to twitch-related reafference; in contrast, reafference from wake movements failed to trigger M1 activity due to sensory gating at the ECN (Tiriac and Blumberg, 2016). This pattern persisted through P10. Then, at P11, M1 neurons suddenly exhibited robust responses to wake-related reafference, a developmental “awakening” that, as demonstrated here, results from an upstream change in sensory processing at the ECN. By P12, M1 neurons were also less responsive to twitch-related reafference due to the onset of local inhibitory control. Altogether, these findings establish that M1 begins its functional existence as a sensory structure that undergoes a complex sequence of state-dependent development (Fig. 8). This sensory framework provides a foundation for M1’s later-emerging role in motor control and learning-related plasticity.

Developmental Changes in Reafferent Responses to Twitches

At P8-10, M1 neurons were maximally responsive to twitches. Further, each twitch-responsive M1 neuron within the forelimb representation had a large receptive field, as evidenced by the fact that twitches of just one muscle—the bicep—triggered responses in half of the neurons from which we recorded (Fig. S7A, top). Although many of the remaining neurons were unresponsive to reafference from twitches and wake movements, they were nonetheless responsive to exafferent forelimb stimulation, most likely because the method of stimulation necessarily affects many forelimb muscles

simultaneously (Fig. S7C, left). Thus, we would expect twitches of another forelimb muscle to produce responses in an overlapping subset of M1 neurons (Fig. S7A, bottom).

Similar to spontaneous retinal waves for the developing visual system (Ackman et al., 2012; Hanganu et al., 2006) and spontaneous cochlear activity for the developing auditory system (Tritsch et al., 2007), twitches provide a robust source of proprioceptive input to M1 neurons for early sensorimotor development (Blumberg, 2015). In this regard, there are several features of twitches that make them more suitable than wake movements for guiding activity-dependent development of the sensorimotor system. First, unlike wake movements, twitches are low-amplitude, discrete events that occur against a background of low muscle tone; these features enable individual twitches to provide high-fidelity reafferent signals to the developing brain. Second, twitches occur exclusively and abundantly during active sleep, the predominant behavioral state in early development (Jouvet-Mounier et al., 1970; Kayser and Biron, 2016). Finally, when combined with the inhibition of wake-related reafference in ECN neurons (Tiriac and Blumberg, 2016), which prevents this reafference from being conveyed to M1 neurons, sensory feedback from twitches is the only reliable source of proprioceptive input to M1 neurons before P10.

The percentage of twitch-responsive M1 neurons decreased suddenly and dramatically by P12 (Fig. 4B). At P11, of the responsive M1 neurons, 73% were twitch-responsive; by P12, however, that percentage had decreased to just 24% (Fig. 4C). This decrease in twitch responsiveness is attributable to local inhibition, as disinhibiting M1 using the $GABA_A$ antagonist, bicuculline, restored twitch responsiveness to 71% (Fig. 7D-F). Thus, by P12, sensory inputs to M1 neurons persist beneath a layer of inhibitory control, suggesting that these inputs constitute the latent connections that permit rapid M1 plasticity in adults (Huntley, 1997a; Jacobs and Donoghue, 1991; Peters et al., 2017). Accordingly, we propose that the broad receptive fields of M1 neurons at P8-10 reveal the foundation of M1's sensory framework and the maximal extent of rapid adult plasticity in that structure.

A closer inspection of twitch responses at P12 suggests that cortical inhibition sharpens the receptive fields of M1 neurons. That is, at P12 a smaller percentage of neurons were consistently driven by bicep twitches. This type of inhibitory sharpening—such that neurons are responsive only to preferred stimuli—has been termed the "iceberg effect" (Carandini and Ferster, 2000; Isaacson and Scanziani, 2011; Rose and Blakemore, 1974) and has been demonstrated across several sensory modalities (Liu et al., 2011; Poo and Isaacson, 2009; Wu et al., 2008). Employing this metaphor here, the water level represents the strength of inhibition and the iceberg that sits above the water represents the sensory inputs with sufficient strength to cause M1 neurons to fire. Thus, at P8—before inhibitory interneurons are functional—even the weakest excitatory inputs

can trigger M1 neurons to fire (Fig. S7A, left). In contrast, at P12, with the emergence of inhibitory control, excitatory inputs must exceed the level of inhibition to drive M1 neurons (Fig. S7A, right).

In adults, cortical inhibition is essential for motor map plasticity in M1 neurons (Jacobs and Donoghue, 1991) and preventing changes to inhibitory synapses blocks task-specific motor learning (Chen et al., 2015). Local inhibitory circuits in M1 have also been shown to play a role early in the development of motor control, with strong inhibition blocking motor outflow between P13 and P35 (Young et al., 2012). The present findings, however, are the first to establish that cortical inhibition directly influences sensory responses in M1 neurons.

Developmental Changes in Reafferent Responses to Wake Movements

The robust sensory response of M1 neurons to twitches stands in sharp contrast to their conspicuous silence following wake movements (Fig. 2A, Tiriac et al., 2014)—a silence highlighted further by the sudden influx of wake-movement reafference at P11 (Fig. 2B,C; Fig. 4B). This sensory transition represents a major milestone in the development of the sensorimotor system. Just as neurons in the developing visual system are initially blind to patterned light (Colonnese et al., 2010)—instead relying on retinal waves for early retinotopic development—M1 neurons are initially “blind” to the consequences of wake movements, relying instead on sensory feedback provided by twitches.

What is the functional significance, if any, that M1 neurons do not respond to reafference from wake movements before P11? If there were no such inhibition, sensory feedback from wake movements could drive excessive synchronized activity across M1 neurons. This is because wake movements, compared to twitches, are composed of concurrent activity across multiple muscles. Noting again that at P8 bicep twitches activate half of all neurons in the forelimb representation of M1, wake movements—were they to be conveyed to M1—would likely result in a much larger and more complex sensory signal. If this were to occur, wake movement reafference could weaken somatotopic organization within M1 during a sensitive period of development.

Regardless, for M1 neurons to participate in motor learning, they must eventually be sensitive to feedback from ongoing movements. As demonstrated here, the critical transition in the responsiveness of M1 neurons occurs suddenly between P10 and P12. This transition, along with the emergence of inhibitory modulation, enables complex wake movements to differentially activate populations of M1 neurons (Fig. S7B, right). This wake movement activity is a precursors to the activity of “movement-related” neurons in adult M1 (Hyland, 1998; Komiyama et al., 2010; Peters et al., 2014). Thus, the increase in wake responsiveness of M1 neurons at P12 provides an essential bridge between their sensory activity over the first postnatal week (Tiriac and Blumberg, 2016;

Tiriac et al., 2014) and their sensory activity after M1 has established its motor functions.

Implications of Wake Responsiveness for Motor Production

In adults, the functional importance of wake movement reafference for M1 motor plasticity is well established (Iriki et al., 1989, 1991). However, at P12, neurons in M1 are not yet involved in motor control, and wake-movement reafference cannot promote motor plasticity. This motivates the question: What is the function of wake-movement reafference in M1 neurons during this early period? We hypothesize that sensory responses to subcortically generated wake movements permit the tutoring of M1 neurons to the sensory consequences of movement. We propose that this process is the necessary next step along the path to M1 establishing its role as a motor structure.

To understand how sensory feedback from wake movements could shape M1 neurons to enable motor outflow, we have to consider the factors that prevent motor production in the developing M1. Intracortical microstimulation experiments in rats reveal that although motor outflow in M1 is possible as early as P13, strong cortical inhibition blocks its expression for several additional weeks (Young et al., 2012). Thus, strong inhibition on M1 corticospinal neurons must be overcome for motor outflow to occur. We propose that sensory feedback from wake movements, beginning at P12, is essential to that process. Indeed, in adults, neurons routinely overcome strong inhibition through focal strengthening of excitatory inputs and weakening of inhibitory inputs (Chen et al., 2015). Importantly, although M1 neurons receive a wide diversity of cortical and thalamic inputs, it is their sensory inputs that are needed to produce long-term increases in neuronal responses (Iriki et al., 1989, 1991).

Evolutionary Implications

The traditional designation of primary motor and sensory cortices as exclusively “motor” and “sensory,” respectively, is contradicted by neurophysiological and comparative studies (Asanuma, 1981; Baldwin et al., 2017a; Baldwin et al., 2017b; Cooke et al., 2015; Hatsopoulos and Suminski, 2011; Lende, 1963a; Matyas et al., 2010). Further, such simplifications ignore the realities of thalamocortical loops as well as the ubiquity of descending motor projections from parietal and frontal cortex (Nudo et al., 1995; Sherman, 2016). From a comparative perspective, placental mammals uniformly have an M1, but many marsupials (including the Virginia opossum) do not (Kaas, 2004). Instead, opossums have what has been referred to as a “sensorimotor amalgam” that exhibits a mix of the features of both S1 and M1 as defined in placental mammals (Karlen and Krubitzer, 2007; Lende, 1963a, b, c). This has led to the hypothesis that both S1 and M1 are derived from the same ancestral brain area and that opossums have retained this ancestral state (Beck et al., 1996).

This evolutionary perspective makes predictions about M1. Specifically, even though M1 in rats is highly specialized, its shared evolutionary history with somatosensory cortex suggests that it should develop similarly to other somatosensory areas, including S1. This suggestion is consistent with a developmental-evolutionary perspective, according to which evolution enables phenotypic transformations in cortical structure through alterations in developmental processes (Krubitzer and Dooley, 2013). Thus, earlier in development, M1 and S1 should exhibit more shared features. The demonstration here that M1 exhibits an exclusively sensory framework long before it contributes to motor control is consistent with this perspective.

Conclusion

The present findings strongly support the idea that M1 is built on a sensory framework that scaffolds its later-emerging motor map (Chakrabarty and Martin, 2005; Huntley, 1997b; Keller et al., 1996). Unique to the present investigation, we have identified the role played by self-generated sleep and wake movements in driving M1's somatotopically organized sensory activity. This approach proved critical to characterizing the sensory development of M1 neurons and documenting how emerging cortical inhibition shapes sensory responses. Because the inhibitory network plays such a crucial role in the expression of adult motor plasticity, our findings further suggest that M1's sensory framework lays a foundation for this plasticity in adulthood.

Damage to M1 in adults can cause a profound loss of motor function. After stroke, the current therapeutic approach is to focus primarily on restoring motor control. Alternatively, it has been suggested that therapeutic outcomes for stroke patients would improve if closer attention were paid to also assessing and restoring proprioceptive function (Semrau et al., 2015). This suggestion aligns nicely with the present findings that M1's motor functions rest atop an earlier-developing sensory framework. Moreover, if understanding the mechanisms of normal development can help inform therapies that promote recovery following stroke, as has been suggested (Johnston, 2009; Murphy and Corbett, 2009), then the present results suggest that the degree of early sensory recovery will predict eventual motor recovery and inform therapeutic interventions.

Finally, it should be noted that the early, intimate connection between active sleep and M1 sensory activity continues into adulthood as a connection between active sleep and motor plasticity. For example, in juvenile and adult mice, active sleep appears to critically influence the elimination and stabilization of new dendritic spines in M1 formed in a motor learning task (Li et al., 2017). This function is not restricted to mammals. For example, in finches, consolidation of song motor memories also depends on neural processes during active sleep (Brawn et al., 2010; Deregnaucourt et al., 2005). Such

findings fit within a broader context linking active sleep to developmental plasticity and memory consolidation (Blumberg and Dooley, 2017; Diekelmann and Born, 2010; Dumoulin Bridi et al., 2015; Maquet et al., 2000). Thus, all together, the present findings encourage a new conceptualization of how M1 is functionally organized and how it adapts to and supports learning across the lifespan.

Acknowledgments

We thank Leah Krubitzer, Dylan Cooke, and Greta Sokoloff for helpful comments. This research was supported by grants from the National Institutes of Health (R37-HD081168 to M.S.B. and T32-NS101858 to J.C.D.)

Author Contributions

Conceptualization, J.C.D. and M.S.B.; Methodology, J.C.D. and M.S.B.; Software: J.C.D.; Formal Analysis: J.C.D.; Investigation: J.C.D.; Data Curation: J.C.D.; Writing – Original Draft, J.C.D. and M.S.B.; Writing – Review & Editing, J.C.D. and M.S.B.; Visualization: J.C.D. and M.S.B.; Funding Acquisition, J.C.D. and M.S.B.; Resources, M.S.B.; Supervision, M.S.B.

Declaration of Interests

The authors declare no competing interests.

REFERENCES

Ackman, J.B., Burbridge, T.J., and Crair, M.C. (2012). Retinal waves coordinate patterned activity throughout the developing visual system. Nature *490*, 219-225.

An, S., Kilb, W., and Luhmann, H.J. (2014). Sensory-evoked and spontaneous gamma and spindle bursts in neonatal rat motor cortex. J Neurosci *34*, 10870-10883.

Asanuma, H. (1981). Functional role of sensory inputs to the motor cortex. Progress in Neurobiology *16*, 241-262.

Baldwin, M.K., Cooke, D.F., and Krubitzer, L. (2017a). Intracortical microstimulation maps of motor, somatosensory, and posterior parietal cortex in tree shrews (Tupaia belangeri) reveal complex movement representations. Cereb Cortex *27*, 1439-1456.

Baldwin, M.K.L., Cooke, D.F., Goldring, A.B., and Krubitzer, L. (2017b). Representations of fine digit movements in posterior and anterior parietal cortex revealed using long-train intracortical microstimulation in macaque monkeys. Cereb Cortex, 1-20.

Beck, P.D., Pospichal, M.W., and Kaas, J.H. (1996). Topography, architecture, and connections of somatosensory cortex in opossums: evidence for five somatosensory areas. J Comp Neurol *366*, 109-133.

Ben-Ari, Y., Gaiarsa, J.L., Tyzio, R., and Khazipov, R. (2007). GABA: a pioneer transmitter that excites immature neurons and generates primitive oscillations. Physiol Rev *87*, 1215-1284.

Blumberg, M.S. (2015). Developing sensorimotor systems in our sleep. Curr Dir Psychol Sci *24*, 32-37.

Blumberg, M.S., and Dooley, J.C. (2017). Phantom limbs, neuroprosthetics, and the developmental origins of embodiment. Trends Neurosci *40*, 603-612.

Blumberg, M.S., Sokoloff, G., Tiriac, A., and Del Rio-Bermudez, C. (2015). A valuable and promising method for recording brain activity in behaving newborn rodents. Dev Psychobiol *57*, 506-517.

Boivie, J., and Boman, K. (1981). Termination of a separate (proprioceptive?) cuneothalamic tract from external cuneate nucleus in monkey. Brain Res *224*, 235-246.

Bopp, R., Holler-Rickauer, S., Martin, K.A., and Schuhknecht, G.F. (2017). An ultrastructural study of the thalamic input to layer 4 of primary motor and primary somatosensory cortex in the mouse. J Neurosci *37*, 2435-2448.

Brawn, T.P., Fenn, K.M., Nusbaum, H.C., and Margoliash, D. (2010). Consolidating the effects of waking and sleep on motor-sequence learning. J Neurosci *30*, 13977-13982.

Bruce, I.C., and Tatton, W.G. (1980). Sequential output-input maturation of kitten motor cortex. Exp Brain Res *39*, 411-419.

Campbell, S.K., Parker, T.D., and Welker, W. (1974). Somatotopic organization of the external cuneate nucleus in albino rats. Brain Res *77*, 1-23.

Carandini, M., and Ferster, D. (2000). Membrane potential and firing rate in cat primary visual cortex. J Neurosci *20*, 470-484.

Chakrabarty, S., and Martin, J.H. (2000). Postnatal development of the motor representation in primary motor cortex. Journal of Neurophysiology *84*, 2582-2594.

Chakrabarty, S., and Martin, J.H. (2005). Motor but not sensory representation in motor cortex depends on postsynaptic activity during development and in maturity. J Neurophysiol *94*, 3192-3198.

Chen, S.X., Kim, A.N., Peters, A.J., and Komiyama, T. (2015). Subtype-specific plasticity of inhibitory circuits in motor cortex during motor learning. Nat Neurosci *18*, 1109-1115.

Colonnese, M.T., Kaminska, A., Minlebaev, M., Milh, M., Bloem, B., Lescure, S., Moriette, G., Chiron, C., Ben-Ari, Y., and Khazipov, R. (2010). A conserved switch in sensory processing prepares developing neocortex for vision. Neuron *67*, 480-498.

Cooke, D.F., Stepniewska, I., Miller, D.J., Kaas, J.H., and Krubitzer, L. (2015). Reversible deactivation of motor cortex reveals functional connectivity with posterior parietal cortex in the prosimian galago (Otolemur garnettii). J Neurosci *35*, 14406-14422.

Deregnaucourt, S., Mitra, P.P., Feher, O., Pytte, C., and Tchernichovski, O. (2005). How sleep affects the developmental learning of bird song. Nature *433*, 710-716.

Diekelmann, S., and Born, J. (2010). The memory function of sleep. Nat Rev Neurosci *11*, 114-126.

Dumoulin Bridi, M.C., Aton, S.J., Seibt, J., Renouard, L., Coleman, T., and Frank, M.G. (2015). Rapid eye movement sleep promotes cortical plasticity in the developing brain. Science advances *1*, e1500105.

Fetz, E.E., Finocchio, D.V., Baker, M.A., and Soso, M.J. (1980). Sensory and motor responses of precentral cortex cells during comparable passive and active joint movements. J Neurophysiol *43*, 1070-1089.

Flament, D., Hall, E.J., and Lemon, R.N. (1992). The development of cortico-motoneuronal projections investigated using magnetic brain stimulation in the infant macaque. J Physiol *447*, 755-768.

Georgopoulos, A.P., Kalaska, J.F., Caminiti, R., and Massey, J.T. (1982). On the relations between the direction of two-dimensional arm movements and cell discharge in primate motor cortex. J Neurosci *2*, 1527-1537.

Goldring, S., and Ratcheson, R. (1972). Human motor cortex: sensory input data from single neuron recordings. Science *175*, 1493-1495.

Hanganu, I.L., Ben-Ari, Y., and Khazipov, R. (2006). Retinal waves trigger spindle bursts in the neonatal rat visual cortex. J Neurosci *26*, 6728-6736.

Hatsopoulos, N.G., and Suminski, A.J. (2011). Sensing with the motor cortex. Neuron *72*, 477-487.

Huntley, G.W. (1997a). Correlation between patterns of horizontal connectivity and the extend of short-term representational plasticity in rat motor cortex. Cereb Cortex *7*, 143-156.

Huntley, G.W. (1997b). Differential effects of abnormal tactile experience on shaping representation patterns in developing and adult motor cortex. J Neurosci *17*, 9220-9232.

Hyland, B. (1998). Neural activity related to reaching and grasping in rostral and caudal regions of rat motor cortex. Behav Brain Res *94*, 255-269.

Iriki, A., Pavlides, C., Keller, A., and Asanuma, H. (1989). Long-term potentiation in the motor cortex. Science *245*, 1385-1387.

Iriki, A., Pavlides, C., Keller, A., and Asanuma, H. (1991). Long-term potentiation of thalamic input to the motor cortex induced by coactivation of thalamocortical and corticocortical afferents. J Neurophysiol *65*, 1435-1441.

Isaacson, J.S., and Scanziani, M. (2011). How inhibition shapes cortical activity. Neuron *72*, 231-243.

Jacobs, K.M., and Donoghue, J.P. (1991). Reshaping the cortical motor map by unmasking latent intracortical connections. Science *251*, 944-947.

Jouvet-Mounier, D., Astic, L., and Lacote, D. (1970). Ontogenesis of the states of sleep in rat, cat, and guinea pig during the first postnatal month. Developmental Psychobiology *2*, 216-239.

Kaas, J.H. (2004). Evolution of somatosensory and motor cortex in primates. Anat Rec A Discov Mol Cell Evol Biol *281*, 1148-1156.

Karlen, S.J., and Krubitzer, L. (2007). The functional and anatomical organization of marsupial neocortex: evidence for parallel evolution across mammals. Progress in neurobiology *82*, 122-141.

Karlsson, K.Æ., Gall, A.J., Mohns, E.J., Seelke, A.M.H., and Blumberg, M.S. (2005). The neural substrates of infant sleep in rats. PLoS Biology *3*, 891-901.

Kayser, M.S., and Biron, D. (2016). Sleep and development in genetically tractable model organisms. Genetics *203*, 21-33.

Keller, A., Weintraub, N.D., and Miyashita, E. (1996). Tactile experience determines the organization of movement representations in rat motor cortex. Neuroreport *7*, 2373-2378.

Komiyama, T., Sato, T.R., O'Connor, D.H., Zhang, Y.X., Huber, D., Hooks, B.M., Gabitto, M., and Svoboda, K. (2010). Learning-related fine-scale specificity imaged in motor cortex circuits of behaving mice. Nature *464*, 1182-1186.

Krubitzer, L., and Dooley, J.C. (2013). Cortical plasticity within and across lifetimes: how can development inform us about phenotypic transformations? Frontiers in human neuroscience *7*, 620.

Lende, R.A. (1963a). Cerebral cortex: a sensorimotor amalgam in the marsupiala. Science *141*, 730-732.

Lende, R.A. (1963b). Motor representation of the cerebral cortex of the opossum (Didelphis virginiana). J Comp Neurol *121*, 405-415.

Lende, R.A. (1963c). Sensory representation in the cerebral cortex of the opossum (Didelphis virginiana). J Comp Neurol *121*, 395-403.

Li, W., Ma, L., Yang, G., and Gan, W.B. (2017). REM sleep selectively prunes and maintains new synapses in development and learning. Nat Neurosci *20*, 427-437.

Liu, B.H., Li, Y.T., Ma, W.P., Pan, C.J., Zhang, L.I., and Tao, H.W. (2011). Broad inhibition sharpens orientation selectivity by expanding input dynamic range in mouse simple cells. Neuron *71*, 542-554.

Ludwig, K.A., Miriani, R.M., Langhals, N.B., Joseph, M.D., Anderson, D.J., and Kipke, D.R. (2009). Using a common average reference to improve cortical neuron recordings from microelectrode arrays. J Neurophysiol *101*, 1679-1689.

Maquet, P., Laureys, S., Peigneux, P., Fuchs, S., Petiau, C., Phillips, C., Aerts, J., Del Fiore, G., Degueldre, C., Meulemans, T.*, et al.* (2000). Experience-dependent changes in cerebral activation during human REM sleep. Nat Neurosci *3*, 831-836.

Marcano-Reik, A.J., Prasad, T., Weiner, J.A., and Blumberg, M.S. (2010). An abrupt developmental shift in callosal modulation of sleep-related spindle bursts coincides with the emergence of excitatory-inhibitory balance and a reduction of somatosensory cortical plasticity. Behav Neurosci *124*, 600-611.

Martin, J.H., Engber, D., and Meng, Z. (2005). Effect of forelimb use on postnatal development of the forelimb motor representation in primary motor cortex of the cat. J Neurophysiol *93*, 2822-2831.

Mathis, M.W., Mathis, A., and Uchida, N. (2017). Somatosensory cortex plays an essential role in forelimb motor adaptation in mice. Neuron *93*, 1493-1503 e1496.

Matyas, F., Sreenivasan, V., Marbach, F., Wacongne, C., Barsy, B., Mateo, C., Aronoff, R., and Petersen, C.C. (2010). Motor control by sensory cortex. Science *330*, 1240-1243.

Miri, A., Warriner, C.L., Seely, J.S., Elsayed, G.F., Cunningham, J.P., Churchland, M.M., and Jessell, T.M. (2017). Behaviorally selective engagement of short-latency effector pathways by motor cortex. Neuron *95*, 683-696 e611.

Muller, K., Homberg, V., and Lenard, H.G. (1991). Magnetic stimulation of motor cortex and nerve roots in children. Maturation of cortico-motoneuronal projections. Electroencephalogr Clin Neurophysiol *81*, 63-70.

Nezu, A., Kimura, S., Uehara, S., Kobayashi, T., Tanaka, M., and Saito, K. (1997). Magnetic stimulation of motor cortex in children: maturity of corticospinal pathway and problem of clinical application. Brain & development *19*, 176-180.

Nudo, R.J., Sutherland, D.P., and Masterton, R.B. (1995). Variation and evolution of mammalian corticospinal somata with special reference to primates. J Comp Neurol *358*, 181-205.

Olivier, E., Edgley, S.A., Armand, J., and Lemon, R.N. (1997). An electrophysiological study of the postnatal development of the corticospinal system in the macaque monkey. J Neurosci *17*, 267-276.

Peters, A.J., Chen, S.X., and Komiyama, T. (2014). Emergence of reproducible spatiotemporal activity during motor learning. Nature *510*, 263-267.

Peters, A.J., Liu, H., and Komiyama, T. (2017). Learning in the rodent motor cortex. Annu Rev Neurosci *40*, 77-97.

Poo, C., and Isaacson, J.S. (2009). Odor representations in olfactory cortex: "sparse" coding, global inhibition, and oscillations. Neuron *62*, 850-861.

Rose, D., and Blakemore, C. (1974). Effects of bicuculline on functions of inhibition in visual cortex. Nature *249*, 375-377.

Schroeder, K.E., Irwin, Z.T., Bullard, A.J., Thompson, D.E., Bentley, J.N., Stacey, W.C., Patil, P.G., and Chestek, C.A. (2017). Robust tactile sensory responses in finger area of primate motor cortex relevant to prosthetic control. J Neural Eng *14*, 046016.

Seelke, A.M., and Blumberg, M.S. (2008). The microstructure of active and quiet sleep as cortical delta activity emerges in infant rats. Sleep *31*, 691-699.

Seelke, A.M., Dooley, J.C., and Krubitzer, L.A. (2012). The emergence of somatotopic maps of the body in S1 in rats: the correspondence between functional and anatomical organization. PloS one *7*.

Sherman, S.M. (2016). Thalamus plays a central role in ongoing cortical functioning. Nat Neurosci *19*, 533-541.

Tiriac, A., and Blumberg, M.S. (2016). Gating of reafference in the external cuneate nucleus during wake movements but not sleep-related twitches. eLife.

Tiriac, A., Del Rio-Bermudez, C., and Blumberg, M.S. (2014). Self-generated movements with "unexpected" sensory consequences. Curr Biol *24*, 2136-2141.

Tritsch, N.X., Yi, E., Gale, J.E., Glowatzki, E., and Bergles, D.E. (2007). The origin of spontaneous activity in the developing auditory system. Nature *450*, 50-55.

Wu, G.K., Arbuckle, R., Liu, B.H., Tao, H.W., and Zhang, L.I. (2008). Lateral sharpening of cortical frequency tuning by approximately balanced inhibition. Neuron *58*, 132-143.

Young, N.A., Vuong, J., and Teskey, G.C. (2012). Development of motor maps in rats and their modulation by experience. J Neurophysiol *108*, 1309-1317.

Figure Legends

Figure 1. Experimental Design and Recording Locations

(A) A head-fixed pup was secured to a platform in a stereotaxic apparatus with its limbs dangling freely. Colored dots correspond to the location of the EMGs (forelimb, red; hindlimb, green; nuchal muscle, blue). hl: hindlimb.

(B) Top: Flattened cortical tissue sectioned tangential to the cortical surface and stained for cytochrome oxidase (CO); primary somatosensory cortex (S1) appears darker than the surrounding tissue. Bottom: Boundaries of primary sensory areas from CO-stained tissue, illustrating S1 (red) and primary motor cortex (M1, blue), as well as primary auditory (A1) and visual (V1) cortex.

(C) Magnification of gray inset in (B) showing the somatotopic organization within S1 (red) and M1 (blue).

(D) Magnification of gray inset in (C) showing the location of recording sites (blue bars) within forelimb representation of M1 for each rat from P8 to P12. For 3 pups in which the cortex was sectioned coronally (see Figure S1), the electrode locations were reconstructed on this flattened representation.

Figure 2. Rapid Developmental Change in Sensory Responsiveness of M1 Neurons

(A) Left: Representative data depicting 20-s periods of active sleep (blue) and wake (red), showing forelimb movements, neural activity within the forelimb representation of M1, rectified EMGs from contralateral forelimb and nuchal muscles at P8. Blue tick marks denote behaviorally scored forelimb twitches and red tick marks denote forelimb wake movements. Each row of neural activity represents action potentials of a single neuron. The bottom most neuron, in blue and red, is the neuron represented to the right of the figure. Right, top: Raster sweeps for an individual M1 neuron triggered on twitches (blue) and wake movements (red), with each row showing the activity surrounding a single movement. Right, bottom: Perievent histogram (bin size = 10 ms) showing mean firing rate for this neuron triggered on twitches (blue) and wake movements (red).

(B) Same as in (A) except at P11.

(C) Same as in (A) except at P12.

See also Figure S2.

Figure 3. Modeling Reafferent Responses of M1 Neurons to Twitches and Wake Movements

(A) Gaussian function used to model M1 neural responses to twitches. Based on the model fits for twitch-triggered perievent histograms, we derived estimates of each neuron's baseline firing rate (BL), maximum response (R_{max}), peak time (T_{max}), and half-width at half-height (HWHH).

(B) Gaussian-exponential function used to model M1 neural responses to wake movements. The function's rising phase is a Gaussian function, identical to that in (A). The falling phase is an exponential decay function. Parameters defined as in (A).
(C) Representative perievent histograms and model fits illustrating all four neuron classifications: Twitch-responsive (blue box), unresponsive (gray box), twitch- and wake-responsive (purple box), and wake-responsive (red box). Each neuron's Gaussian fit (blue lines) and Gaussian-exponential fit (red lines) are shown. Fits with adjusted r^2 values less than 0.35 are shown with a dotted line and fits with an adjusted r^2 value greater than 0.35 are shown with a solid line.

Figure 4. Developmental Shift in the Population Characteristics of Sensory Responses of M1 Neurons
(A) Scatterplot of each M1 neuron's adjusted r^2 value for twitches (y-axis) and wake movements (x-axis) across age. Background color illustrates the classification of neurons within that region of the scatterplot.
(B) Mean ($\pm$ SEM) adjusted r^2 value for twitches (blue) and wake movements (red) for responsive M1 neurons at each age. * significant difference from previous day ($P < 0.005$). † significant difference from two days prior ($P < 0.005$).
(C) Percentage of neurons classified as wake-responsive (red), twitch- and wake-responsive (purple), and twitch-responsive (blue) at each age.
See also Figures S3 and S4.

Figure 5. State-Dependent ECN Sensory Activity
(A) Model of ECN neuronal activity in response to twitches and wake movements at P9, as proposed previously (Tiriac and Blumberg, 2016). For twitches, neurons in the ECN convey the twitch-related reafference to downstream structures, including thalamus and, ultimately, M1. For wake movements, a motor copy inhibits the ECN neuron, preventing the conveyance of reafference to downstream structures.
(B) Proposed model of ECN neuronal activity in response to twitches and wake movements at P12. The ECN's gating of twitch-related reafference is identical to that at P9. However, at P12, we propose that wake-related reafference ceases to be gated in the ECN, permitting this reafference to be conveyed to downstream structures.
(C) Left: Representative data depicting 20-s periods of active sleep (blue) and wake (red), showing forelimb movements, multi-unit activity (MUA), sorted neural activity from the forelimb representation of M1, and rectified EMGs from ipsilateral forelimb and nuchal muscles in a P9 rat. Right, top: Raster sweeps for an individual ECN neuron triggered on twitches (blue) and wake movements (red), with each row showing the activity surrounding a single movement. Right, bottom: Perievent histogram (bin size = 10 ms) showing mean firing rate for this neuron triggered on twitches (blue) and wake movements (red).

(D) Same is in (C), except for a P12 rat.
See also Figure S5

Figure 6. Developmental Onset of Wake-Related Reafference in the ECN

(A) Scatterplot of each ECN neuron's adjusted r^2 value for twitches (y-axis) and wake movements (x-axis) for P9 (left) and P12 (right) rats. Background color illustrates the classification of neurons within that region of the scatterplot.
(B) Mean (± SEM) adjusted r^2 value for twitches (blue) and wake movements (red) for ECN neurons recorded from P9 and P12 rats. * significant difference from P9 ($P < 0.025$).
(C) Percentage of ECN neurons that were wake-responsive (red), twitch- and wake-responsive (purple), and twitch-responsive (blue) at both ages.

Figure 7. Local Disinhibition of M1 Neurons at P12 Unmasks Twitch-Related Activity

(A) Proposed model of inhibitory modulation of reafferent activity of M1 neurons after twitches and wake movements. At this age, reafference from both twitches and wake movements is conveyed to M1 neurons, but local inhibitory circuits only block reafference from twitches.
(B) Left, Top: Coronal section showing CO staining of S1/M1 boundary. Left, Bottom: Fluorescent image of the same section showing the spatial extent of bicuculline diffusion (blue). White arrow indicates the location of a single electrode shank in M1 (red).
Right, Top: Diagram of the histological sections to the left showing the boundaries of S1 and M1, the laminar structure of each area, and a reconstruction of the location of the microsyringe needle immediately lateral to the recording electrode. Right, Top: Experimental timeline.
(C) Recording site (black bars) and diffusion boundaries (blue ovals) for all 6 saline injections (top) and 5 bicuculline injections (bottom). The 6^{th} bicuculine injection is shown in (B). All recording sites were within the forelimb representation of M1; diffusion boundaries were largely restricted to M1.
(D) Top: Adjusted r^2 values for twitches (y-axis) and wake movements (x-axis) for each isolated M1 neuron before (Pre) and after (Post) injection of saline. Bottom: Same as above, but for bicuculline group.
(E) Mean (± SEM) adjusted r^2 values for twitches (blue) and wake movements (red) before (Pre) and after (Post) injections of saline or bicuculline at P12. * significant difference from Pre ($P < 0.0125$).

(F) Percentage of M1 neurons that were wake-responsive (red), twitch- and wake-responsive (purple), and twitch-responsive (blue) during the Pre and Post periods in the saline and bicuculline groups.

Figure 8. Summary of Developmental Changes in Reafferent Processing

(A) Left: At P8, twitch-related reafference is conveyed to downstream structures, including M1. Right: At P12, twitch-related reafference reaches cortex, but is inhibited by interneurons.

(B) Left: The ECN blocks wake-related reafference from reaching downstream structures, resulting in no wake movement response at this age. Right: At P12, the ECN no longer selectively inhibits sensory feedback from wake movements, permitting the conveyance of reafference to M1.

STAR METHODS

CONTACT FOR REAGENT AND RESOURCE SHARING

Further information and requests for resources and reagents should be directed to, and will be fulfilled by, the lead contact, James Dooley (james-c-dooley@uiowa.edu).

EXPERIMENTAL MODEL AND SUBJECT DETAILS

For recordings in the forelimb representation of M1, a total of 49 male and female Sprague-Dawley Norway rats (*Rattus norvegicus*) at P8-12 were used (n=7-15 at each age; mean = 15.4 neurons per pup, s.d. = 7.24). In a subset of these animals, dual recordings were performed in the ECN or the forelimb representation of primary somatosensory cortex (S1) as part of a different study. For ECN recordings, a total of 13 male and female rats were used (n=6 at P8-9; n=7 at P11-12; mean = 3.3 neurons per pup, s.d. = 1.79). For M1 recordings before and after injection of saline or bicuculline, a total of 12 male and female rats were used at P12 (n=6 per group; mean = 17.2 neurons per pup, s.d. = 4.39). See Table S1 for addition information.

Pups were born to mothers housed in standard laboratory cages (48 x 20 x 26 cm) in a room with a 12:12 light dark schedule. Food and water were available ad libitum. Expecting mothers were checked at least once daily for pups. The day of birth was considered P0. If necessary, on or before P3 litters were culled to 8 pups (typically with equal numbers of males and females). Littermates were never assigned to the same experimental groups. All experiments were conducted in accordance with the National Institutes of Health (NIH) Guide for the Care and Use of Laboratory Animals (NIH Publication No. 80-23) and were approved by the Institutional Animal Care and Use Committee of the University of Iowa.

METHOD DETAILS

Surgery

For all studies, pups were prepared for neurophysiological recording using methods similar to those described previously (Blumberg et al., 2015; Tiriac and Blumberg, 2016; Tiriac et al., 2014). On the day of testing, a pup with a visible milk band was removed from the litter. Under isoflurane anesthesia (3-5%; Phoenix Pharmaceuticals, Burlingame, CA), custom-made bipolar hook electrodes (epoxy coated, 0.002 inch diameter; California Fine Wire, Grover Beach, CA) were implanted into the *biceps brachii* muscle of the forelimb, the *extensor digitorum longus* muscle of the hindlimb, and the nuchal muscle for electromyographic (EMG) recordings. Wires were secured using a small amount of collodion. A stainless-steel ground wire (uncoated, 0.002 inch

diameter; California Fine Wire, Grover Beach, CA) was implanted transdermally on the dorsum. The pup was injected with carprofen (5 mg/kg subcutaneously; Putney, Portland, ME) and a rectangular section of skin was removed above the skull. After topical application of bupivicane as an analgesic (Pfizer, New York, NY), the skull was cleaned and dried. Vetbond (3M, Minneapolis, MN) was applied to the skin around the perimeter of the exposed skull and a custom-built head-fix apparatus was secured to the skull using cyanoacrylate adhesive. To limit mobility during recovery, the pup was wrapped in gauze and maintained at thermoneutrality (35 °C) in a humidified incubator for at least 1 h. The entire surgery lasted approximately 15 min.

After recovery, the pup was lightly reanesthetized (2-3% isoflurane) in a stereotaxic apparatus. A small hole (diameter = 1.8 mm) was drilled in the skull using a trephine drill bit (1.8 mm; Fine Science Tools, Foster City, CA), leaving the dura intact. In experiments where saline or bicuculine were also injected into M1, a larger 2.7 mm trephine was used to allow placement of both the electrode and the microsyringe needle. For M1 forelimb recordings, the coordinates were: AP: 0.8-1.2 mm anterior to bregma; L: 1.7-2.0 mm. For ECN recordings, the coordinates were: AP: 3.0 to 3.2 mm posterior to lambda; L: 1.6 to 2.0 mm. Small holes were also made bilaterally in occipital cortex to allow insertion of the thermocouple and combined reference/ground electrode. This procedure lasted approximately 5 min, after which anesthesia stopped and the exposed dura was covered with mineral oil to prevent drying. The pup was then transferred and secured to a different stereotaxic apparatus within a Faraday cage where its torso was supported on a narrow platform and its limbs dangled freely on both sides (Fig. 1A). Brain temperature was monitored using a fine-wire thermocouple (Omega Engineering, Stamford, CT) inserted into occipital cortex contralateral to the M1 recording site. The pup acclimated for at least 1 h until its brain temperature reached at least 36 °C and it was cycling between sleep and wake, at which time electrophysiological recordings began.

Electrophysiological Recordings

The EMG bipolar hook electrodes and corresponding ground electrode were connected to a differential amplifier (Tucker-Davis Technologies, Alachua, FL). A chlorinated Ag/Ag-Cl ground electrode (0.25 mm diameter; Medwire, Mt. Vernon, NY) was inserted into occipital cortex ipsilateral to the M1 recording site or contralateral to the ECN recording site. For M1 recordings, data were acquired using 16-channel silicon depth electrodes (Fig. S1A bottom; Model A4x4-3mm-100-125-177-A16; NeuroNexus, Ann Arbor, MI). The electrodes were inserted 700–1400 µm beneath the cortical surface. For ECN recordings, custom-designed 16-channel silicon depth electrodes were used (Fig. 4C; NeuroNexus). The electrode was angled caudally 14-16° and lowered 3.7-4.2 mm beneath the surface of the brain. EMG and neural signals were sampled at approximately 1 kHz and 25 kHz, respectively. Bandpass filters were applied to EMG

(300-5000 Hz) and neural (0.1 Hz-12.5 kHz) signals. A notch filter was also used. Before insertion of a silicon electrode, it was coated with fluorescent DiI (Vybrant DiI Cell-Labeling Solution; Life Techologies, Grand Island, NY) for subsequent histological verification of placement. Depth of insertion was monitored using a hydraulic micromanipulator (FHC, Bowdoinham, ME).

General Experimental Procedure

The M1 electrode was slowly lowered while manually stimulating the contralateral forelimb (or the ipsilateral forelimb for ECN recordings) using a small wooden probe until a neural response was detected. Once responsive neurons were identified, the electrode settled in place for at least 15 min to allow stabilization of neural signals before the start of data collection. Recording sessions comprised continuous collection of neurophysiological and EMG data for 30 min. During acquisition, the experimenter monitored the pup's behavior and used two digital markers to record the occurrence of active-sleep twitches and wake movements of the forelimb of interest. As described previously (Karlsson et al., 2005), myoclonic twitches are phasic, rapid, and independent movements of the skeletal muscles against a background of muscle atonia (Fig. 2, Fig. 5C,D). In contrast, wake movements are high-amplitude, coordinated movements occurring against a background of high muscle tone (Fig. 2, Fig. 5C,D). Throughout the recording session, the behavior of the animal was also recorded using a digital camera (Prosilica GC; Allied Vision, Exton, PA) whose signal was acquired and synchronized with the electrophysiological record (DV2; Tucker-Davis Technologies). After 30 min of uninterrupted behavioral data collection, exafferent neural responses were recorded by gently stimulating the forelimb using a wooden probe. At least 20 stimulations were presented at an interval of one stimulation every 5-10 s.

Pharmacological Disinhibition of Forelimb M1

Pups were prepared for M1 recording as described above. In addition, a Hamilton microsyringe (1 µL; Hamilton, Reno, NV) was inserted immediately lateral to the recording electrode (see Fig. 6B). The recording session began with a 30-min baseline period (Pre) followed by a 30- to 90-min diffusion/acclimation period and a 30-min recording period (Post). A total volume of 0.25-0.3 µL of bicuculline (2 mM; Sigma-Aldrich, St. Louis, MO) or saline was injected slowly (0.1 µL/min). Fluoro-Gold (4%; Fluorochrome, Denver, CO) was also included in both saline and bicuculline injections to enable subsequent visualization of drug diffusion (Fig. 6B). Immediately after injection of bicuculline, M1 multiunit activity became synchronized, with all neurons bursting every 300-400 ms. The period of this activity varied across pups and the Post period did not begin until normal multiunit activity was observed. The bursts of synchronized activity rarely occurred after the Post period began; when they did, activity within ±100

ms of the burst was not included in the analysis. Only neurons that were held throughout the recording session were included in the final analysis.

Histology

At the end of data collection, the pup was euthanized with an overdose of 10:1 ketamine/xylazine (>0.08 mg/kg) and perfused with phosphate-buffered saline (PBS), followed by 4% paraformaldehyde. The brain was immediately extracted and post-fixed in 4% paraformaldehyde for at least 24 h. Next, 24-48 h before the brain was sectioned, it was transferred to a 20% solution of sucrose in PBS until it was no longer buoyant in solution.

For brains used for M1 recordings, and in all but 3 pups, the cortical hemispheres were dissected apart from the underlying tissue, including the hippocampus and basal ganglia, and flattened between glass slides separated by 1.5 mm copper-coated zinc spacers (United States Mint, Washington, D.C.) for 5-30 min. Small weights (10 g) were used to apply light pressure to the top glass slide. The flattened cortex was then sectioned tangential to the pial surface. In the remaining 3 pups, the cortex was sectioned coronally to confirm electrode depth (see Fig. S1). Regardless of the plane of section, cortex was sectioned at 80 µm using a freezing microtome (Leica Microsystems, Buffalo Grove, IL). To confirm the location of medullary recordings in the ECN, the medulla was sectioned coronally at 80 µm. Electrode location and drug diffusion were initially visualized and photographed in free-floating sections at 2.5X or 5X using a fluorescent microscope and digital camera (Leica Microsystems).

Cortical sections were stained for cytochrome oxidase (CO), which has been shown in developing rats as young as P5 to reliably delineate primary sensory areas, including S1 (Seelke et al., 2012). Briefly, cytochrome C (3mg per 10mL solution; Sigma-Aldrich), catalase (2 mg per 10 mL solution; Sigma-Aldrich) and 3,3'-diaminobenzidine tetrahydrochloride (DAB; 5 mg per 10mL solution; Spectrum, Henderson, NV) were dissolved in a 1:1 dilution of PB-H_2O and distilled water. Sections were developed in well plates on a shaker at 35-40 °C for 3-6 h after which they were washed and mounted. Medullary sections were stained with cresyl violet.

Stained sections were again photographed at 2.5X or 5X magnification, combined into a single composite image (Microsoft Image Composite Editor; Microsoft, Redmond, WA), and the location of the electrode was visualized in relation to areal, nuclear, or laminar boundaries of the stained tissue (Fig. 1, Fig. 7, Fig. S1, Fig. S5,).

QUANTIFICATION AND STATISTICAL ANALYSIS

All analyses and statistical tests for neural and behavioral data were performed using custom-written MATLAB routines (version 2017a; Mathworks, Natick, MA) and Spike2

software (version 8; Cambridge Electronic Design). Alpha was set at 0.05 for all analyses, unless otherwise stated. Normally distributed data were tested for significance using a one-way ANOVA or t-test. Non-normally distributed data (adjusted r^2 values, model fit parameters) were tested for significance using the Kruskal-Wallis nonparametric test or the Mann-Whitney U test. When Kruskal-Wallis tests were significant, post hoc pairwise comparisons across age were performed using the Mann-Whitney U test, with significance values adjusted for multiple comparisons using the Bonferroni procedure. Reported group data in text are always mean ± standard error (SEM), unless otherwise stated. Box plots represent the 25^{th}, 50^{th} (median), and 75^{th} percentiles. Datapoints were considered outliers if they differed from the median by more than 3 standard deviations.

Behavioral State and Movement Classification

As described previously (Tiriac et al., 2014), EMG signals and digitally scored behavior were used to identify behavioral states. EMG signals were rectified and smoothed at 0.001 seconds. Periods of wake were identified by dichotomizing all available EMGs into periods of high tone (indicative of wake) and atonia (indicative of sleep). As the nuchal muscle EMG typically shows chronic tone during wake periods, it was used most often for classifying sleep and wake states. Active sleep was characterized by the occurrence of myoclonic twitches against a background of muscle atonia (Seelke and Blumberg, 2008). For each EMG, a twitch threshold was set that was at least 3X greater than baseline. The initiation time of twitches was recorded as the first data point where the rectified EMG signal exceeded this threshold. When a twitch was identified, a subsequent twitch of that same muscle was only counted if it occurred at least 300 ms after the first; this procedure protected against duplicative analysis of neural data.

For identification of forelimb wake movements, the forelimb EMG was rectified and smoothed at 0.01 s. The baseline wake EMG value was then calculated and a threshold of 5X this baseline value was then determined. To be considered a wake movement, the smoothed EMG waveform had to be preceded by a period of low tone, rise and remain above the wake threshold for at least 300 ms, and then either be (1) behaviorally scored as a forelimb wake movement during data collection or (2) identified as a forelimb wake movement by reviewing the video recording. The wake movement's initiation time was set as the first data point where the rectified and smoothed EMG waveform exceeded the threshold. This criterion for the initiation of wake movements was established in preliminary experiments by observing video of pup forelimb movements simultaneously with EMG records; in this way, we could identify the time at which changes in the EMG waveform most reliably predict limb movements on the video.

Our criteria ensured that only the first wake movement in a bout of wake movements was used as a trigger for assessing associated neural activity (although all wake movements were scored behaviorally). Thus, the counts of triggered wake movements underestimated the actual number of wake movements across the 30-min recording periods (Fig. S2A).

Using experimenter-recorded digital markers, EMG signals, and video, the timing of exafferent stimulation was also identified.

Multiunit Activity and Spike Sorting

All electrode channels were filtered for multiunit activity (MUA; 500-5000 Hz). Spike sorting was performed offline using Spike2. Once filtered, movement artifact was still visible in some medullary recordings; to remove this artifact we created a virtual reference for each channel out of the mean waveform of the remaining channels (Ludwig et al., 2009). This virtual reference was then subtracted from each channel's multiunit waveform.

Spike sorting was performed on channels with visually identifiable spiking activity that exceeded at least 2X baseline using template matching and principal component analysis in Spike2. Putative neurons were visually investigated and waveforms were excluded as outliers when they were more than 3.5 standard deviations beyond the mean of a given template. To ensure that two channels did not identify the same putative neuron, cross-correlations of all putative neurons were graphed and investigated; duplicate neurons were excluded when necessary.

Movement-Related Neural Activity

The relationship between neural response type and firing rate was assessed as follows: First, using either twitches or wake movements as triggers, perievent histograms (2000-ms windows; 10-ms bins) of neural activity were constructed. The average firing rate (in spikes per second, sps) was calculated for each bin and plotted. Next, the twitch-triggered perievent histogram was fit to the following Gaussian model:

$$R(t) = BL + \left(R_{max} \cdot e^{-\frac{(t-t_{max})^2}{2c^2}} \right)$$

with baseline term BL in sps, maximum response term R_{max} in sps, maximum time term t_{max} in seconds, and Gaussian width term c, where the half-width at half-height $(HWHH) = \sqrt{2\ln(2)}c$ in seconds.

The rising phase of the neuron's wake response was fit to the same Gaussian function above, whereas the fall was fit to an exponential decay function, centered around the time of maximal response:

$$R(t) = \begin{cases} t \leq t_{max}, & BL + \left(R_{max} \cdot e^{-\frac{(t-t_{max})^2}{2c^2}}\right) \\ t > t_{max}, & BL + \left(R_{max} \cdot e^{-\lambda \cdot (t-t_{max})}\right) \end{cases}$$

with the same terms as for the Gaussian model, but with the addition of the exponential term λ, proportional to the half-life $t_{1/2}$, where $t_{1/2} = \frac{\ln(2)}{\lambda}$

The adjusted r^2 of these models was then calculated and the neuron was considered responsive to a given movement (twitch or wake) if it had an adjusted $r^2 > 0.35$. Thus, every neuron was classified as one of four types: unresponsive, twitch-responsive, wake-responsive, or twitch- and wake-responsive depending on its fit to these models.

For responsive neurons, these models also provided estimates of baseline firing rate, peak time, peak firing rate, half-width at half-height, and, for wake movements, half-life.

Neural Percentages

The percentage of responsive neurons ($P(R_{total})$) was calculated to be the sum of neurons with either r^2_{twitch} or r^2_{wake} greater than 0.35, divided by the total number of neurons (N), as follows:

$$P(R_{total}) = \left(\frac{\sum\left(N(r^2_{twitch} > 0.35) | N(r^2_{wake} > 0.35)\right)}{\sum N}\right) * 100$$

The percentage of twitch-responsive, wake-responsive, and twitch- and wake-responsive neurons were then calculated relative to the total number of responsive neurons.

Percentage of Movements with a Response

For both twitches and wake movements, triggered movements did not always result in a neural response. Thus, we quantified the percentage of movements (with each twitch or wake movement being an individual trial) that resulted in more activity than would be expected during baseline activity. First, we used the models described above to determine the expected response start time (t_{start}) and end time (t_{end}) relative to the movement time for each neuron. Next, we computed the response duration ($t_{response}$), such that:

$$t_{response} = t_{end} - t_{start}$$

To calculate the total response for each movement (R_{trial}), we then summed the total number of action potentials (S) within this response window for each movement:

$$R_{trial} = \left(\sum_{t_{end}}^{t_{start}} S \right)$$

Next, we determined the proportion of movement trials ($P(R_{trial\,raw})$) with more action potentials than what would be expected at the baseline firing rate:

$$P(R_{trial\,raw}) = \frac{\sum \left(R_{trial} > \left(BL * t_{response} \right) \right)}{N_{movements}}$$

Because the baseline action potentials were not normally distributed, we then calculated the number of action potentials during a period of baseline activity starting 2 s before the movement (R_{BL}):

$$R_{BL} = \left(\sum_{t=(-2+t_{response})}^{t=-2} S \right)$$

and determined the proportion of baseline periods of duration $t_{response}$ that exceeded the expected baseline firing rate:

$$P(R_{BL}) = \frac{\sum \left(R_{BL} > \left(BL * t_{response} \right) \right)}{N_{movements}}$$

Finally, we subtracted the proportion of trials where the baseline firing rate exceeded its expected value ($P(R_{BL})$) from the proportion of trials with a response above baseline ($P(R_{trial\,raw})$), and multiplied this value by 100 to determine the percentage of trials with a response exceeding the baseline firing rate ($P(R_{trial})$):

$$P(R_{trial}) = \left(\frac{P(R_{trial\,raw}) - P(R_{BL})}{1 - P(R_{BL})} \right) * 100$$

DATA AND SOFTWARE AVAILABILITY

The custom Matlab code used to fit data to models will be made available upon request.

Figure S1. M1 Recording Locations in Coronal Perspective
Related to Figure 1.

(A) Upper: Illustration of a rat brain showing the location of primary somatosensory cortex (S1; red), the recording location in the forelimb representation of M1 (1) and the location of the ground electrode in occipital cortex (2). Grey box shows the rostrocaudal location of the coronal sections in (B). Lower: Diagram of the 4-shank electrode used for M1 recordings.

(B) Left: Coronal section stained for CO showing the electrode location (black arrow). Right: Diagram of the coronal section showing somatotopic representations in S1 and the laminar structure of S1 and M1. Recordings were performed at a depth of 700-1200 µm, with the recording sites targeted at the thalamic recipient layer (i.e., at the layer 3/5 boundary). lj: lower jaw.

Figure S2. Frequency and Kinematics of Twitches and Wake Movements Across Age
Related to Figure 2.

(A) Mean (± SEM) number of triggered twitches (blue) and wake movements (red) across all pups over 30 min of recording at each age. Dots indicate mean values for each individual pup. There was no effect of age on the number of wake movements, but there was for twitches. † significant difference from two days prior ($P < 0.005$).

(B) Mean rectified EMGs for twitch (light-blue lines) and wake movements (light-red lines) for each pup at each age. Bold blue and red lines represent median values. Arrows denote movement onset. For twitch EMG records, insets are magnifications of the associated gray regions.

Figure S3. Mean Perievent Histograms by Age, Neuron Response Classification, and Triggered Event
Related to Figure 4.

(A) Mean perievent histograms (in spikes per s, sps) for all neurons at each age, for each response classification, and for each type of triggered event category. Baseline firing rates were subtracted from individual responses before calculating means. Each column identifies the type of triggered event (twitch, blue; wake movement, red; exafferent stimulation, green) denoted by the black arrows. For each colored grid, the color of the background indicates the response classification of the neurons being averaged (twitch, blue; twitch and wake, purple, wake, red; unresponsive, gray). Thus, a blue line against a blue background represents the mean twitch response (blue line) of all twitch-responsive neurons (blue background) at that age, and a blue line against a gray background represents the mean twitch response (blue line) of all unresponsive neurons (gray background) at that age.

(B) Stacked bar plot of the percentage of neurons at each age classified as unresponsive (gray), twitch-responsive (blue), twitch- and wake-responsive (purple) and wake-responsive (red). White numbers within the stacked bar plots indicate the number of neurons identified for that response type at that age.

Figure S4. Developmental Refinement of Twitch-Responsive Neurons Related to Figure 4.

(A) Box plots of baseline activity for twitch-responsive (upper, blue) and wake-responsive (lower, red) neurons. A significant Kruskal-Wallis for twitch-responsive neurons ($H_{(4,238)}$ = 50.3, P < 0.0001) and wake-responsive neurons ($H_{(4,169)}$ = 34.0, P < 0.0001) permitted pairwise comparisons. Alpha was set to 0.05, with the Bonferroni adjustment used to correct for multiple comparisons. * significant difference from previous day (P < 0.005). † significant difference from two days prior (P < 0.005).

(B) Same as in (A), but for peak height. Twitch-responsive neurons showed a significant effect of age ($H_{(4,238)}$ = 78.5, P < 0.0001).

(C) Same as in (A), but for half-width at half-height. For wake-responsive neurons, half-width at half-height refers only to the rising (Gaussian) part of the function. Twitch-responsive neurons showed a significant effect of age ($H_{(4,238)}$ = 55.4, P < 0.0001).

(D) Same as in (A), but for exponential half-life (only applicable to wake-responsive neurons).

(E) Same as in (A), but for peak response time. Both twitch-responsive neurons ($H_{(4,238)}$ = 108.6, P < 0.0001) and wake-responsive neurons ($H_{(4,169)}$ = 16.4, p = 0.0025) showed a significant effect of age.

(F) Percentage of twitches and wake movements that resulted in increased neural activity in relation to the activity expected during baseline. The percentage of twitches that produced a neural response showed a significant effect of age ($H_{(4,238)}$ = 33.66, P < 0.0001).

Figure S5. ECN Recording Location and Representative Neural Activity Related to Figure 5.

(A) Left, Top: Nissl-stained coronal section showing electrode location in the ECN (arrow). Right, Top: Nuclear boundaries of ECN, cuneate nucleus, and spinal trigeminal tract (sp5) in relation to section at left. Left, Bottom: Location of the recording electrode (1) and ground electrode (2), with the gray box indicating the plane of coronal section above. Green oval is the approximate extent of the ECN. Right, Bottom: Electrode used to record ECN neural activity.

(B) Electrode locations for ECN recordings in P9 (gray) and P12 (black) rats. Asterisk denotes recording shown in (A). Single electrodes represent the electrode location of cases where ECN neurons were identified on a single electrode shank; two electrodes

bound together with a line are cases where ECN neurons were identified on both electrode shanks.
(C) Perievent histograms of firing rate (spikes per s, sps) for representative ECN neurons at P9 (top) and P12 (bottom) triggered on twitches (blue) and wake movements (red). Conventions as in Figure 3C.

Figure S6. Representative M1 Neural Activity Before and After Injection of Saline or Bicuculline at P12
Related to Figure 7.
Perievent histograms of firing rate (spikes per s, sps) for representative M1 neurons triggered on twitches (blue) and wake movements (red) before (Pre) and after (Post) injections of saline (left) or bicuculline (right). Conventions as in Figure 3C.

Figure S7. Hypothesized Developmental Changes in Sensory Processing of M1 Neurons
Related to Figure 8.
(A) Afferent projections to neurons within the forelimb representation of M1 arising from two forelimb muscles at P8 (left) and P12 (right). Gray M1 neurons are inactive. At P8, when Muscle X (top row; yellow) or Muscle Y (bottom row; blue) twitches, reafference results in activation of a partially overlapping subset of neurons, regardless of synaptic strength. At P12, inhibitory interneurons (red) prevent ascending inputs with weak synapses from activating M1 neurons, resulting in twitch-related activation of only that neuron with the strongest synapse (yellow or blue).
(B) During a wake movement, multiple muscles are recruited. At P8 (left), none of the ascending inputs from Muscles X or Y activate M1 neurons (gray) due to upstream sensory gating at the ECN. At P12 (right), when sensory gating at the ECN no longer occurs, contemporaneous activation of Muscles X and Y results in excitation of only those M1 neurons (green) that receive inputs from both muscles so as to exceed cortical inhibition (red).
(C) As with wake movements, exafferent stimulation recruits multiple muscles. At P8 (left), all of the ascending inputs from Muscles X or Y activate M1 neurons (yellow, green, blue) because the ECN does not gate exafference at this age. At P12 (right), when inhibitory control has emerged (red interneurons), contemporaneous stimulation of Muscles X and Y results in excitation of only those M1 neurons (green) that receive inputs from both muscles so as to exceed cortical inhibition (red).

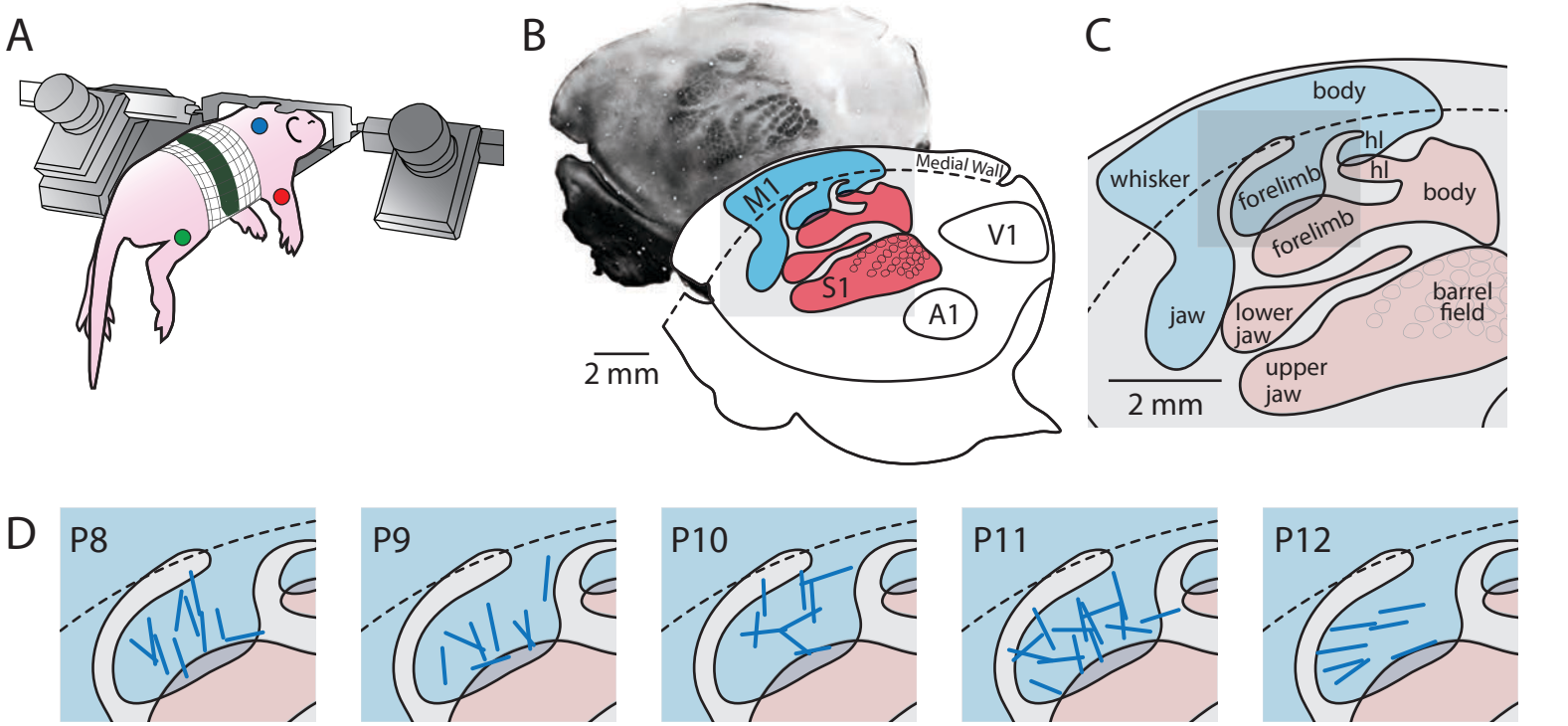
A
B
C
D
Medial Wall
M1
S1
V1
A1
2 mm
body
whisker
forelimb
hl
hl
body
forelimb
jaw
lower jaw
barrel field
upper jaw
2 mm
P8
P9
P10
P11
P12

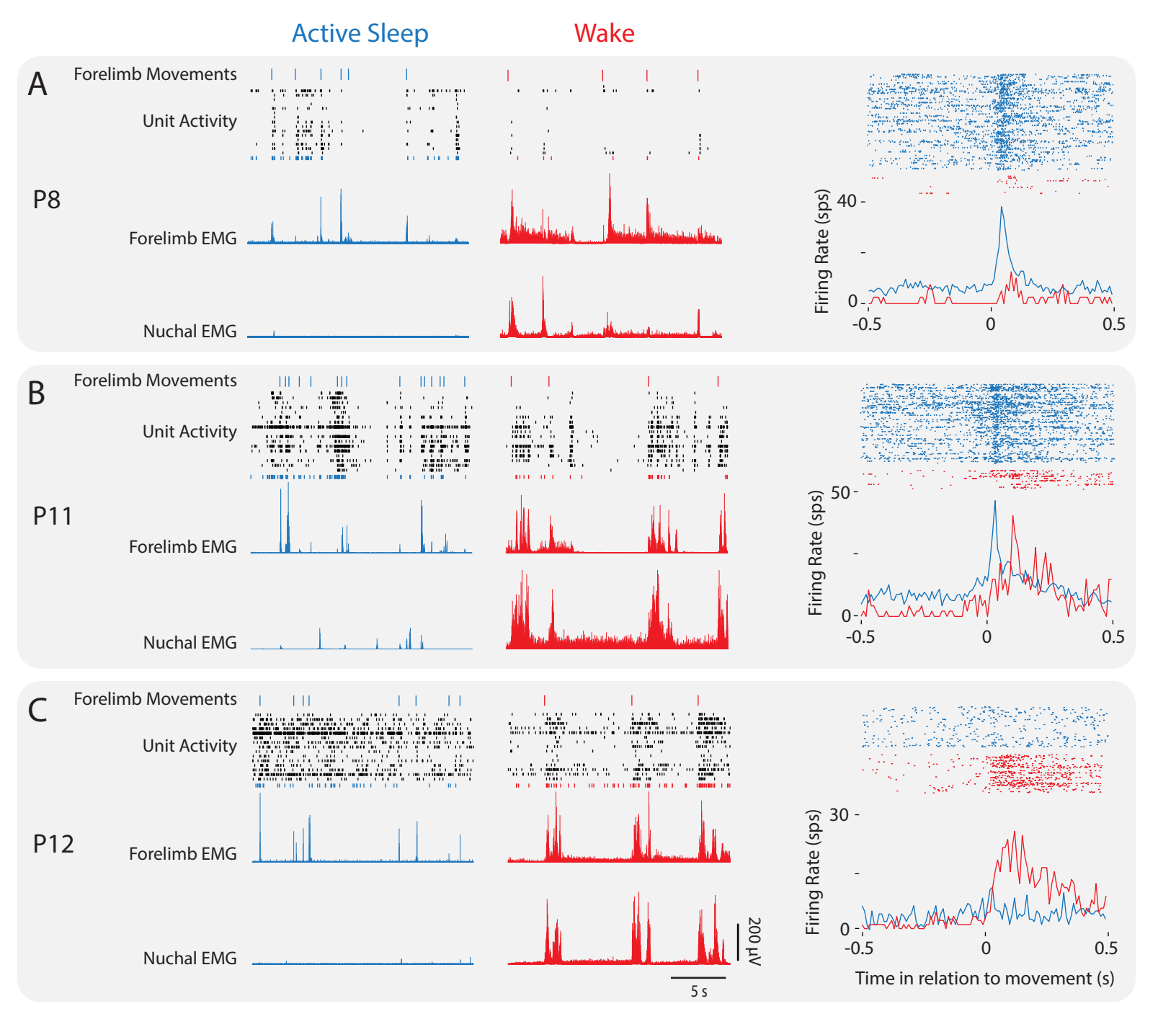
Active Sleep
Wake
A
Forelimb Movements
Unit Activity
P8
Forelimb EMG
Nuchal EMG
Firing Rate (sps)
40
0
-0.5
0
0.5
B
Forelimb Movements
Unit Activity
P11
Forelimb EMG
Nuchal EMG
Firing Rate (sps)
50
0
-0.5
0
0.5
C
Forelimb Movements
Unit Activity
P12
Forelimb EMG
Nuchal EMG
200 µV
5 s
Firing Rate (sps)
30
0
-0.5
0
0.5
Time in relation to movement (s)

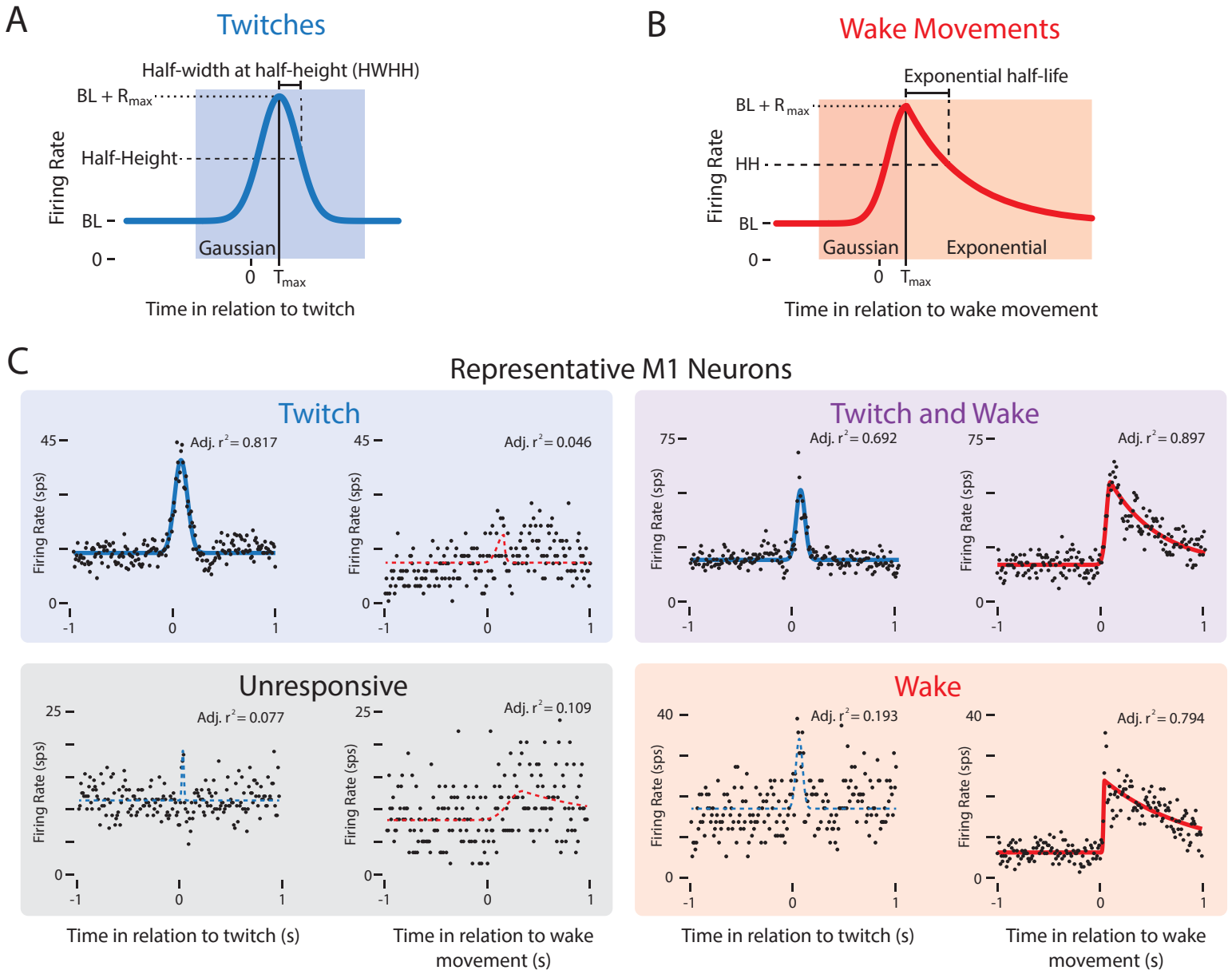
A
Twitches
Half-width at half-height (HWHH)
BL + Rmax
Half-Height
BL
0
Firing Rate
Gaussian
0
Tmax
Time in relation to twitch
B
Wake Movements
Exponential half-life
BL + Rmax
HH
BL
0
Firing Rate
Gaussian
Exponential
0
Tmax
Time in relation to wake movement
C
Representative M1 Neurons
Twitch
Adj. r2 = 0.817
Adj. r2 = 0.046
Twitch and Wake
Adj. r2 = 0.692
Adj. r2 = 0.897
Unresponsive
Adj. r2 = 0.077
Adj. r2 = 0.109
Wake
Adj. r2 = 0.193
Adj. r2 = 0.794
Firing Rate (sps)
Time in relation to twitch (s)
Time in relation to wake movement (s)
Time in relation to twitch (s)
Time in relation to wake movement (s)

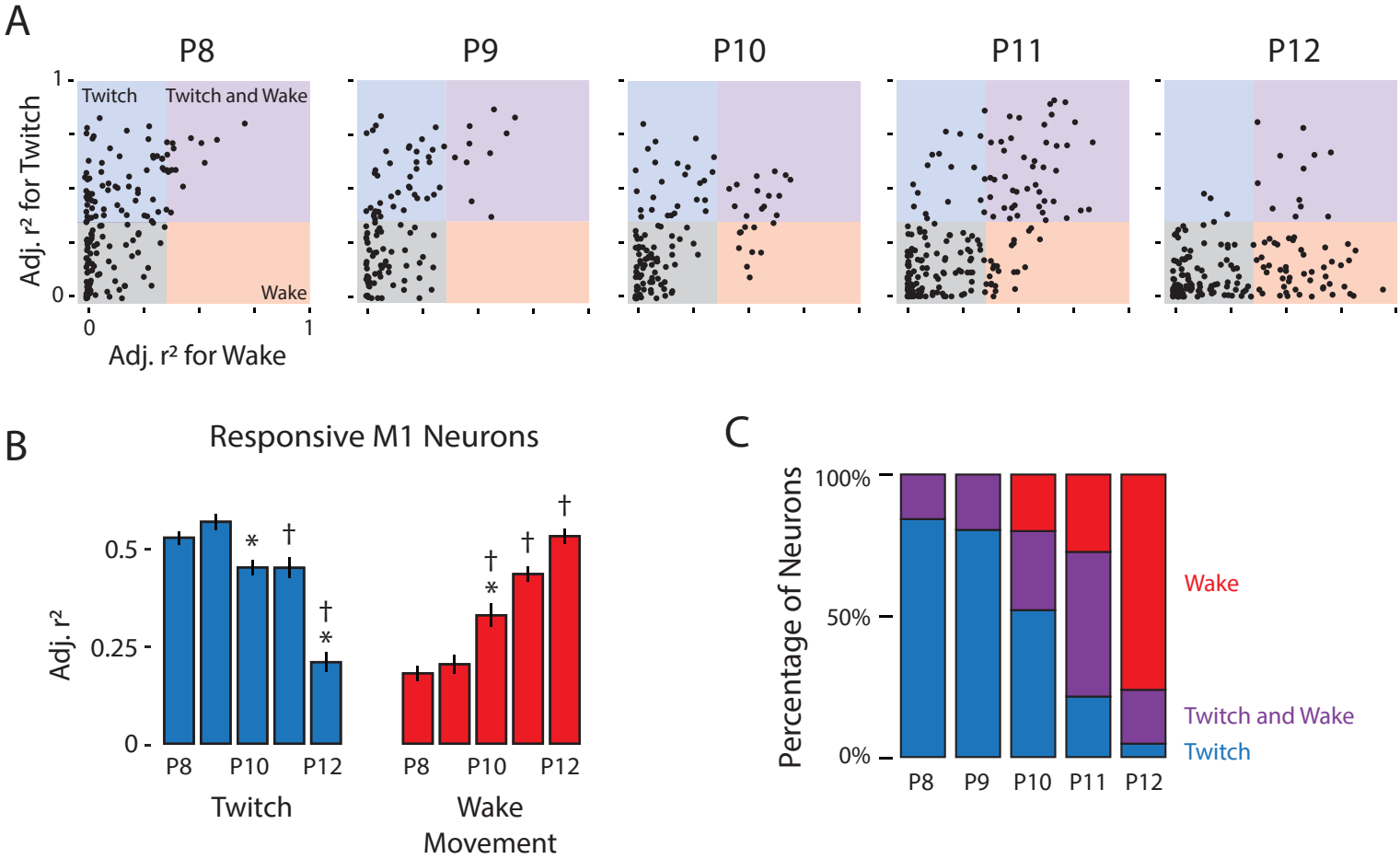
A
P8
P9
P10
P11
P12
Twitch
Twitch and Wake
Wake
Adj. r² for Twitch
Adj. r² for Wake
1
0
0
1
B
Responsive M1 Neurons
Adj. r²
0.5
0.25
0
P8
P10
P12
Twitch
Wake
Movement
C
Percentage of Neurons
100%
50%
0%
P8
P9
P10
P11
P12
Wake
Twitch and Wake
Twitch

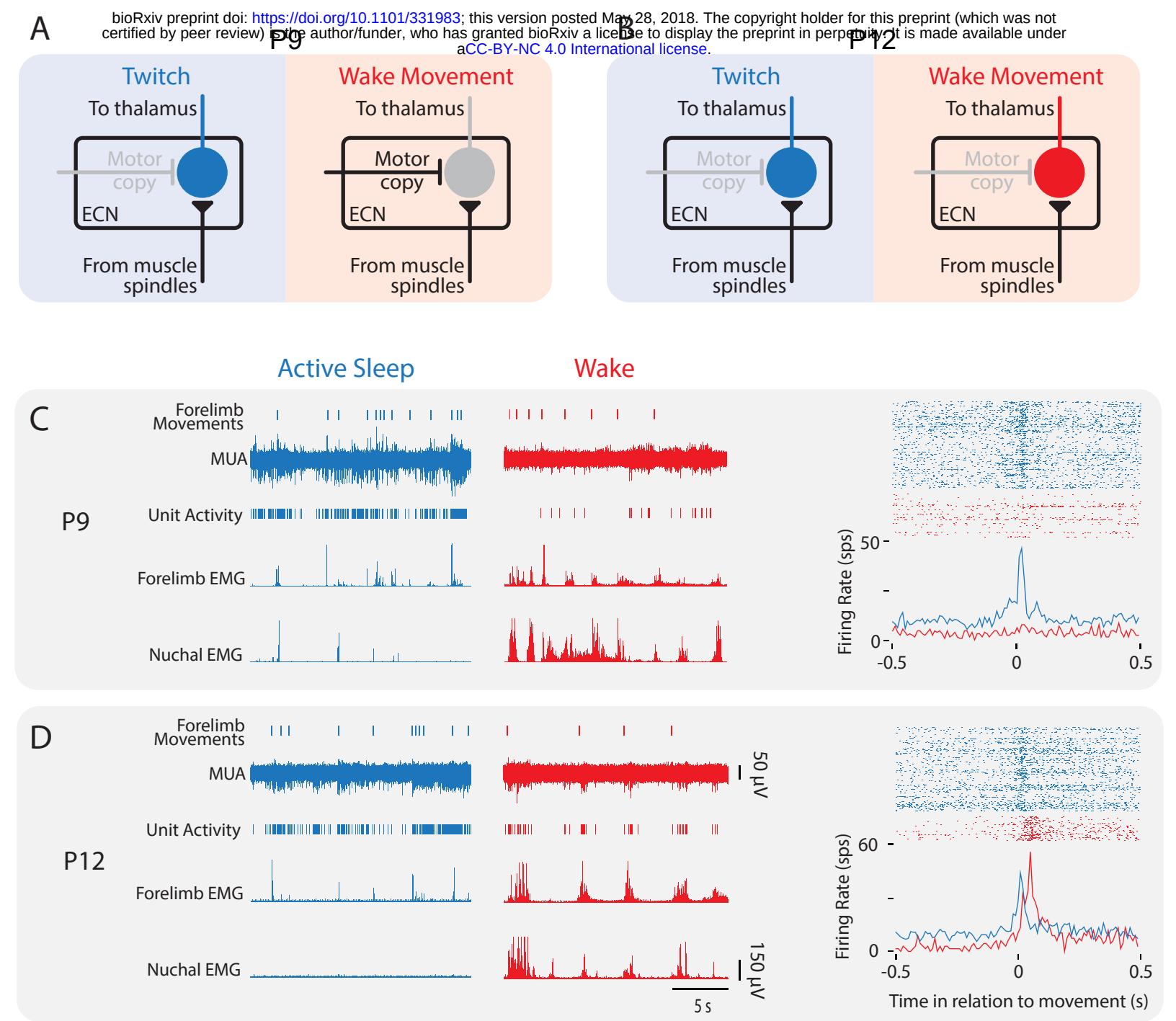

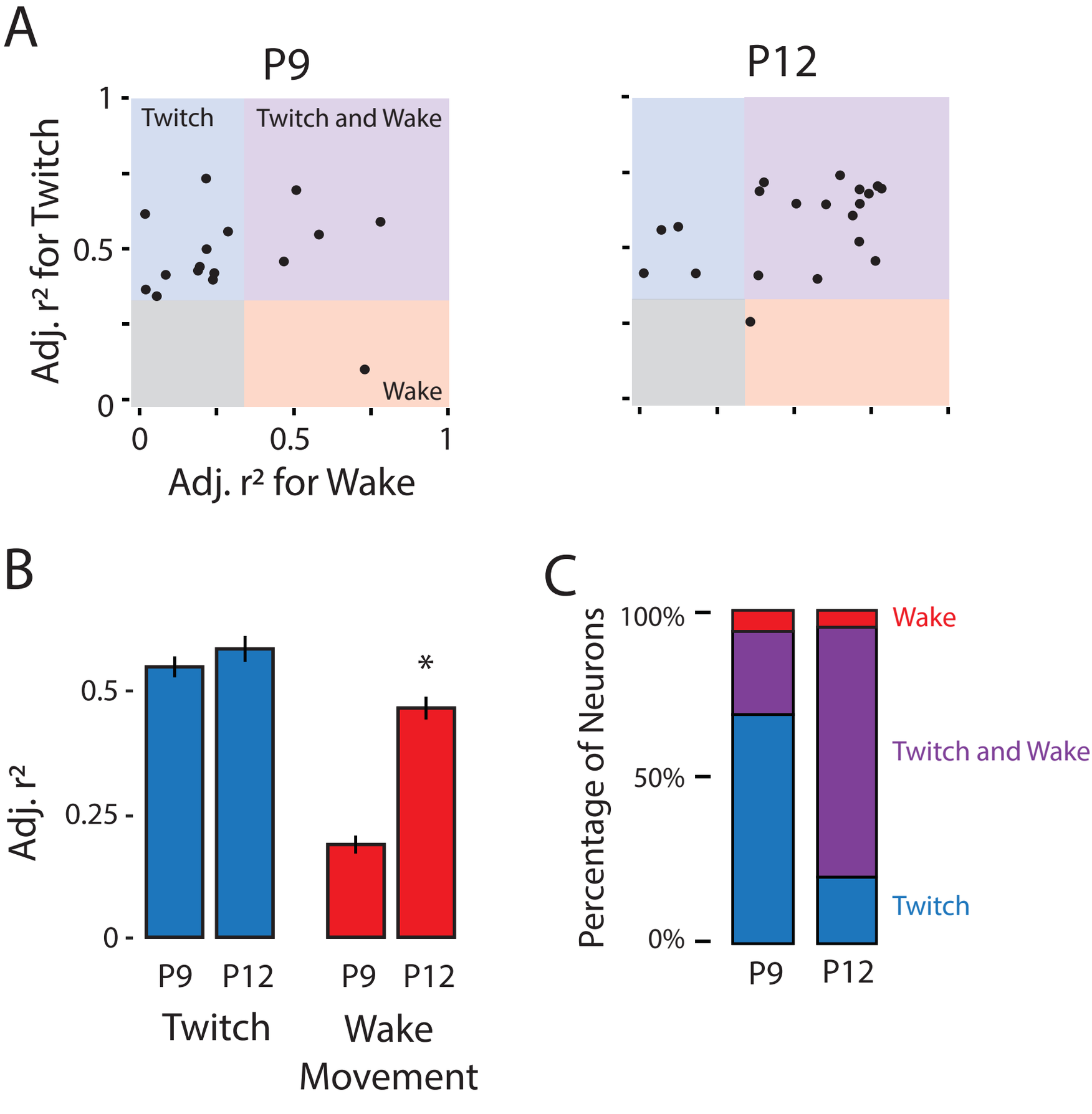
A
P9
P12
Twitch
Twitch and Wake
Wake
Adj. r² for Twitch
Adj. r² for Wake
0
0.5
1
B
Adj. r²
0
0.25
0.5
*
P9
P12
P9
P12
Twitch
Wake
Movement
C
Percentage of Neurons
100%
50%
0%
Wake
Twitch and Wake
Twitch
P9
P12